

Fast kinetic Monte Carlo simulation of strained heteroepitaxy in three dimensions

Chi-Hang Lam and M.T. Lung

Department of Applied Physics, Hong Kong Polytechnic University, Hung Hom, Hong Kong, China

Leonard M. Sander

*Michigan Center for Theoretical Physics, Department of Physics,
Randall Laboratory, University of Michigan, Ann Arbor, MI 48109-1120, USA*

(Dated: August 31, 2021)

Accelerated algorithms for simulating the morphological evolution of strained heteroepitaxy based on a ball and spring lattice model in three dimensions are explained. We derive exact Green's function formalisms for boundary values in the associated lattice elasticity problems. The computational efficiency is further enhanced by using a superparticle surface coarsening approximation. Atomic hoppings simulating surface diffusion are sampled using a multi-step acceptance-rejection algorithm. It utilizes quick estimates of the atomic elastic energies from extensively tabulated values modulated by the local strain. A parameter controls the compromise between accuracy and efficiency of the acceptance-rejection algorithm.

PACS numbers:

Epitaxial growth techniques enable deposition of a dislocation-free thin film on a substrate of a different material with a mismatched lattice constant. For film-substrate combinations such as Ge/Si, InAs/GaAs and InAs/InP, arrays of three-dimensional (3D) coherent islands self-assemble spontaneously beyond certain film thicknesses under appropriate growth conditions [1, 2, 3, 4]. These studies are of much current interest since they are expected to find applications in future microelectronic devices.

One of the most widely studied examples is Ge/Si(100) with a 4% lattice misfit. Relatively flat islands called pre-pyramids start to emerge at 3 monolayers (MLs) of Ge coverage [5, 6, 7]. Upon further deposition, they quickly grow into truncated pyramids bounded by four (105) facet planes on the sides and subsequently into fully grown pyramids which are also called hut islands. Upon still further deposition, they become dome islands bounded mainly by (113) facet planes. Finally, large dislocated islands appear. For the closely related alloy variant $\text{Si}_{1-x}\text{Ge}_x/\text{Si}(100)$ with a generally lower $4x\%$ misfit, the development is rather similar and goes through stages characterized by ripples, hut islands, dome islands and finally dislocated islands [8, 9, 10]. The structures are however larger and each transition is postponed to occur at a larger film thickness. The islands are also more closely packed.

Islands self-assemble because they can relieve the elastic stress in the heteroepitaxial films. There is theory for island formation that emphasizes nucleation. It suggests that islands must overcome an energy barrier associated with a critical size so that the elastic energy gained can balance the extra surface energy cost [11]. The theory is reasonably consistent with experiments at relatively high misfit. At low misfit, the critical island size and hence the energy barrier are expected to increase and make nucleation prohibitively difficult. Island formation mechanisms which do not have a barrier then offer a more

promising explanation. For example, according to the Asaro-Tiller-Grinfeld (ATG) theory [12, 13, 14], strained surfaces are unstable at sufficiently long wavelengths. Therefore, shallow ripples first develop from small random initial perturbations and then into islands. For this mechanism to operate the temperature must be above the surface roughening transition point. This seems to be the case for the (100) plane of a $\text{Si}_{1-x}\text{Ge}_x$ which is not a true facet at the experimentally relevant temperatures [15, 16].

Direct simulation of the growth of a strained film is much more challenging computationally than for the unstrained case because of the long-range nature of elastic interactions. Early kinetic Monte Carlo simulations in two dimensions (2D) based on ball and spring lattice models by Orr et. al [17], Barabasi [18], and Khor and Das Sarma [19] have successfully observed island formation on strained films at sufficiently high misfits. The mechanism is consistent with the nucleation picture. These simulations focus on the high misfit regime because islands can then be small enough to be computationally manageable. More recently, much enhanced computational efficiency has been achieved using an exact Green's function method for the elasticity problem of surface atoms. Using also a superparticle coarsening approximation and a hopping acceptance-rejection sampling method, a much wider range of morphologies for both high and low temperature regimes characterized respectively by instability and nucleation roughening mechanisms in both 2D [20, 21] and 3D [22, 23] have been explored. Another advanced approach for the elasticity problem based on the fast Fourier transform and a multi-grid method applied respectively to the substrate and film has also been derived [24, 25]. All of these studies work for general film morphologies. Alternatively, one can limit the study to the evolution of only shallow structures and solve the elastic problem using the half-space Green's function in the small-slope approximation

[26, 27].

Other computational approaches offer different compromises between accurate representation of the physics and computational efficiency. For instance, continuum simulations using driven diffusion equations with the elastic energy term obtained using finite element or similar methods are computationally less intensive. The ATG instability is readily demonstrated [28] and effects of surface anisotropy [29] as well as island coarsening [30] can be studied in 3D. The importance of alloy segregation [31] and formation of more complicated structures [32] have also been studied recently. Nevertheless, fluctuations in the atomic scale and lattice discreteness are not accounted for and hence island nucleation and growth at sub-roughening transition temperatures cannot be studied. Also, off-lattice models are more realistic and island formation can be simulated at moderate length scales in 2D [33]. Moreover, molecular models using realistic semiconductor atomic potentials have provided better understanding of island stress distribution [34] and facet structures [35] in static calculations. Finally, first principles calculations focus on the statics of fewer atoms but are able to provide important estimates for the surface energies of relevant facets bounding the islands [36, 37, 38].

Thus kinetic Monte Carlo methods based on lattice models are unique in allowing large scale dynamic simulations for studying properties for which atomic discreteness is important while fine details of the atomic potential and surface energies are of limited qualitative impacts. In the following, we will explain in detail the algorithms used in Ref. [22] which has enabled some of the most efficient lattice based kinetic simulations in 3D reported in the literature.

I. MODEL

The model parameters of our 3D ball and spring model for strained heteroepitaxy are appropriate to the $\text{Si}_{1-x}\text{Ge}_x/\text{Si}(001)$ system. It is based on a cubic lattice with a substrate lattice constant $a_s = 2.715\text{\AA}$ so that a_s^3 gives the correct atomic volume in crystalline silicon. The lattice constant a_f of the film material is related to the lattice misfit $\epsilon = (a_f - a_s)/a_f$ which has a compositional dependence $\epsilon = 0.04x$. Nearest and next nearest neighboring atoms are directly connected by linear elastic springs with force constants $k_1 = 2eV/a_s^2$ and $k_2 = k_1$ respectively. The shear moduli in (100) and (110) directions are given by $G_{100} = k_2/a_s$ and $G_{110} = (k_1 + k_2)/2a_s$. They are equal for our choice of k_1 and k_2 and this leads to better isotropy of our system. The elastic couplings of adatoms with the rest of the system are weak and are completely neglected for better computational efficiency. Solid-on-solid conditions and atomic steps limited to at most one atom high are assumed. Every topmost atom in the film can hop to a different random topmost site within a neighborhood of $l \times l$ columns with equal probability. We put $l = 17$.

Decreasing the hopping range does not alter our results significantly. The hopping rate Γ_m of a topmost atom m follows an Arrhenius form:

$$\Gamma_m = R_0 \exp \left[-\frac{n_{1m}\gamma_1 + n_{2m}\gamma_2 - \Delta E_m - E_0}{k_B T} \right] \quad (1)$$

Here, n_{1m} and n_{2m} are the numbers of nearest and next nearest neighbors of atom m . We take $\gamma_1 = 0.085eV$ and $\gamma_2 = \gamma_1/2$. Single-layer terrace edges along (100) and (110) directions have energies per unit length given by $(\gamma_1 + 2\gamma_2)/a_s$ and $\sqrt{2}(\gamma_1 + \gamma_2)/a_s$ which are close to each other. The energy ΔE_m is the difference in the strain energy E_s of the whole lattice at mechanical equilibrium when the site is occupied versus unoccupied. We put $E_0 = 0.415eV$ and $R_0 = 2D_0/(\sigma a_s)^2$ with $D_0 = 3.83 \times 10^{13} \text{\AA}^2 s^{-1}$ and $\sigma^2 = l^2/6$. This gives the appropriate adatom diffusion coefficient for silicon (100) [39]. Note that the hopping rates defined in Eq. (1) following Ref. [17] obey detailed balance in contrast to those adopted in Refs. [18, 19, 24]. While not necessarily essential in non-equilibrium situations considered here, detailed balance adds to the reliability of our results.

The main numerical challenge of our simulation lies on the repeated calculations of the elastic energies ΔE_m of topmost atoms in order to compute the hopping rates Γ_m from Eq. (1). The elasticity problem can be formulated as follows. First, we note that the strain in a flat film is homogeneous [2]. This provides a convenient reference position with displacement $\vec{u}_i = 0$ for every atom i . From Hooke's law after applying linearization, the force on atom i exerted by a directly connected neighbor j is

$$\vec{f}_{ij} = -\mathbf{K}_{ij}(\vec{u}_i - \vec{u}_j) + \vec{b}_{ij} \quad (2)$$

where the symmetric matrix $\mathbf{K}_{ij} = k_{ij}\hat{n}_{ij}\hat{n}_{ij}^t$ is the modulus tensor and $\vec{b}_{ij} = (l_{ij}^0 - l_{ij})\mathbf{K}_{ij}\hat{n}_{ij}$ arises from the homogeneous stress in flat films. The spring constant k_{ij} equals either k_1 or k_2 for tangential or diagonal connections respectively. The unit column vector \hat{n}_{ij} points from the unstrained lattice position of atom j towards that of atom i and t denotes transpose. Furthermore, l_{ij}^0 and l_{ij} are respectively the natural and homogeneously strained spring lengths which follow easily from a_s and ϵ . Mechanical equilibrium requires $\sum_j \vec{f}_{ij} = 0$ for each atom i . This leads to a large set of equations coupling the displacements \vec{u}_i of *all* the atoms. Conventionally, this large set of equations is solved directly using approximation schemes [17, 19]. The solution then gives the elastic energy stored in every spring and their sum gives the total elastic energy E_s of the whole system in mechanical equilibrium. Calculating E_s twice with and without the atom m and comparing the values give ΔE_m . This has to be done in principle for every topmost atom m after every successful atomic hop involving non-adatoms. Fast algorithms are hence indispensable.

Our Green's function method to be explained in the next section is a variant of the boundary integral method; it directly calculates the displacement of the surface

atoms only. We show here that this is already sufficient for calculating the elastic energy E_s of the whole system. First, a surface atom is defined as one which has at least one spring missing. There are hence more surface atoms than topmost atoms. Consider virtual forces which adiabatically increase from 0 to $\sum_{j'} \vec{b}_{jj'}$ applied to every surface atom j where j' is summed over all missing atoms which could have been directly connected to j . These forces push all atoms from their mechanical equilibrium positions to their homogeneously strained lattice positions, i.e. a displacement $-\vec{u}_j$. The virtual work done, $W > 0$, is given by

$$W = -1/2 \sum_{jj'} \vec{b}_{jj'} \cdot \vec{u}_j \quad (3)$$

It equals the difference $E_s^0 - E_s$. Here, E_s^0 denotes the strain energy of the homogeneously strained lattice and can be straightforwardly computed by simple bond counting. Therefore, the elastic energy E_s of the whole system is given by

$$E_s = E_s^0 + \frac{1}{2} \sum_{jj'} \vec{b}_{jj'} \cdot \vec{u}_j \quad (4)$$

which depends only on the positions of the surface atoms [40].

II. EXACT GREEN'S FUNCTION METHODS

We now explain in detail the Green's function method which reduces the elasticity problem into one involving explicit consideration of only the surface atoms. This leads to a greatly reduced set of equations and dramatically reduces the computational burden. It is analogous to boundary integral methods [41]. Either full-space or half-space Green's functions defined on an extended lattice with regular boundaries can be used. More importantly, it is exact for arbitrary morphologies. This is in sharp contrast to half-space Green's functions in the small slope approximation which are often applied [11, 26, 27].

First, as a mathematical construct, we enlarge the lattice representing arbitrary morphology by adding *ghost* atoms with similar elastic properties to form an extended lattice with regular boundaries. Unphysical couplings are hence introduced but can be exactly cancelled. The precise method to achieve this is not unique. We will first explain a displacement-based Green's function method which has been applied in our simulations [20, 21, 22]. For completeness, we will also introduce closely related force-based and hypersingular displacement-based Green's function formalisms. They are not currently adopted but have distinct properties which may lead to other applications in the future. For all these formalisms, we take periodic boundary conditions in lateral directions and fixed boundary conditions at the bottom of the substrate as dictated by the lattice model. For the top layer

in the extended lattice, we adopt fixed boundary conditions but free boundary conditions are equally good since all their influences will be exactly cancelled anyway.

A. Displacement-based formalism

A real surface atom j experiences an unphysical force $\vec{f}_{jj'}$ by a directly connected ghost atom j' given by Eq. (2). To cancel all unphysical forces by the ghost atoms, we apply an exactly opposite external force

$$\vec{f}_j^e = - \sum_{j'} \vec{f}_{jj'} \quad (5)$$

to atom j where the sum is over all ghost atom j' directly connected to the real atom j . Noting that the elastic properties of the real and ghost atoms are identical, we apply Eq. (2) and obtain

$$\vec{f}_j^e = \sum_{j'} [\mathbf{K}_{jj'} (\vec{u}_j - \vec{u}_{j'}) - \vec{b}_{jj'}] \quad (6)$$

This introduces the unknown displacements $\vec{u}_{j'}$ for the ghost atoms. In this formalism, instead of solving for their values, we apply another external force $\vec{f}_{j'}^e$ on every ghost surface atom j' which pushes all ghost atoms back to the homogeneously strained positions with $\vec{u}_{j'} \equiv 0$. The force $\vec{f}_{j'}^e$ consists of a term $-\sum_j \vec{f}_{j'j}$ which exactly cancels the spring forces by the real atoms j as well as a term $\sum_j \vec{b}_{j'j}$ which provides the necessary homogeneous stress. Using Eq. (2) and $\vec{u}_{j'} \equiv 0$, we get

$$\vec{f}_{j'}^e = - \sum_j \mathbf{K}_{jj'} \vec{u}_j \quad (7)$$

where j is summed over all real surface atoms directly connected to j' . Equation (6) also reduces to

$$\vec{f}_j^e = \sum_{j'} (\mathbf{K}_{jj'} \vec{u}_{j'} - \vec{b}_{jj'}) \quad (8)$$

With the external forces \vec{f}_j^e and $\vec{f}_{j'}^e$ on the real and ghost surface atoms respectively, the real lattice is exactly decoupled from the ghost atoms. Therefore, the problem defined on the extended lattice with the applied forces is identical to the original physical one. It is hence legitimate to calculate the displacement \vec{u}_i of any real atom i based on the extended lattice being acted on by the external forces, i.e.

$$\vec{u}_i = \sum_j \mathbf{G}_{ij} \vec{f}_j^e + \sum_{j'} \mathbf{G}_{ij'} \vec{f}_{j'}^e \quad (9)$$

where \mathbf{G} denotes the lattice Green's function for the *extended* lattice. An important point is that \mathbf{G} is *independent of the film morphology* and can be computed numerically prior to the start of the simulation. Substituting Eqs. (7) and (8) into Eq. (9), we arrive at the

main equation of the displacement-based Green's function approach

$$\vec{u}_i = \sum_{jj'} [(\mathbf{G}_{ij} - \mathbf{G}_{ij'})\mathbf{K}_{jj'}\vec{u}_j - \mathbf{G}_{ij}\vec{b}_{jj'}] \quad (10)$$

where the double sum is over all pairs of directly connected real and ghost surface atoms j and j' respectively. Although Eq. (10) holds for any atom i , restricting i to only real surface atoms, Eq. (10) now constitutes a greatly reduced set of equations from which the values of \vec{u}_i for all surface atoms are obtained numerically using the bi-conjugate gradient method. The elastic energy E_s of the whole system then follows immediately from Eq. (4).

Our simulations do not require calculating the displacements of the bulk atoms, which can be a time consuming task. Nevertheless, to obtain \vec{u}_i for a bulk atom i for consistency checks or for the purpose of presentation, we simply apply Eq. (10) and substitute the displacements of the surface atoms to its R.H.S. Figure 1 shows the calculated displacements of both surface and bulk atoms in the cross-section of a film from a small scale 3D simulation. Another interesting property of Eq. (10) is that the long-range nature of the elastic interactions is reflected in the coupling coefficient $(\mathbf{G}_{ij} - \mathbf{G}_{ij'})\mathbf{K}_{jj'}$ which decays as $1/r^2$ in 3D at large r where r is the distance between atoms i and j . Therefore, the coupling of the displacements of the surface atoms is also long-ranged as expected and should not be casually truncated. They can be efficiently accounted for using a coarsening scheme discussed later. This exact Green's function approach has been motivated by lattice patching and bond breaking considerations. The derivation is particularly simple and intuitive. We have since learned that it is a lattice analog of the boundary integral method for continuum elasticity [41]. It is also closely related to an earlier result derived algebraically using Dyson's equation [42].

B. Force-based formalism

We now explain a closely related but distinct Green's function approach for the elastic problem which has yet been applied in our simulations. The displacements for the ghost surface atoms $\vec{u}_{j'}$ in Eq. (6) are put to zero by applying an additional set of external forces in the previous discussion. Alternatively, they can be formally solved without resorting to new forces. Equation (6) is first rewritten as

$$\vec{f}_i^e = \sum_{i'} [\mathbf{K}_{ii'}(\vec{u}_i - \vec{u}_{i'}) - \vec{b}_{ii'}] \quad (11)$$

where the sum is over all ghost atoms i' directly connected to the real atom i . Now, $\vec{u}_{i'}$ no longer vanishes in general. Similar to Eq. (9), the displacements of both real and ghost atoms i and i' can be expressed using

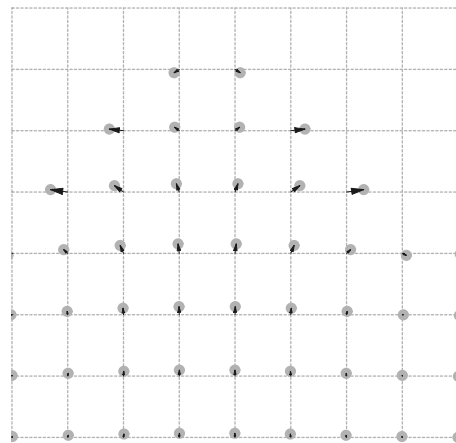


FIG. 1: Cross-section of a strained film in 3D with a rough surface from a small scale simulation. Each arrow represents the displacement vector \vec{u}_i of an atom i from its homogeneously strained lattice position indicated by the dotted lines.

the only external forces \vec{f}_j^e now present and the Green's function \mathbf{G} for the extended lattice as follows

$$\vec{u}_i = \sum_j \mathbf{G}_{ij} \vec{f}_j^e \quad (12a)$$

$$\vec{u}_{i'} = \sum_j \mathbf{G}_{i'j} \vec{f}_j^e \quad (12b)$$

where the sums are over all real surface atoms j . Substituting the displacements into Eq. (11) gives

$$\vec{f}_i^e = \sum_{j i'} \mathbf{K}_{ii'} (G_{ij} - G_{i'j}) \vec{f}_j^e - \sum_{i'} \vec{b}_{ii'} \quad (13)$$

This is the main set of equations in the force-based formalism. They are to be solved numerically to obtain the external forces \vec{f}_i^e for all real surface atoms i . The displacement \vec{u}_i for the real surface atoms and hence the elastic energy E_s can then be readily calculated using Eqs. (12a) and (4) respectively.

The coupling coefficient in Eq. (13) also decays as $1/r^2$ with the distance r as in the previous displacement-based case. For the whole procedure in calculating E_s , from both operation counting and actual numerical implementation, the computational efficiency of this force-based formalism is similar to the previous displacement-based formalism. However, the main variable \vec{f}_i^e here is not a physical quantity and apparently admits no intuitive coarsening scheme, in contrast to that for the displacement-based case to be discussed in Section III. Thus we have not pursued this approach further. We are not aware of any similar formalism reported in the literature.

C. Hyper-singular displacement-based formalism

By explicitly demanding mechanical equilibrium of the real surface atoms, the displacement based formalism in Sec. II A can be further developed into another form analogous to the hyper-singular boundary integral method [41]. For a real surface atom i , equilibrium implies $\sum_k \vec{f}_{ik} = 0$ where k is summed over all directly connected real neighbors of i , which are not necessarily surface atoms. Applying Eq. (2), we get

$$\sum_k [\mathbf{K}_{ik}(\vec{u}_i - \vec{u}_k) - \vec{b}_{ik}] = 0 \quad (14)$$

We now apply Eq. (10) twice to express both \vec{u}_i and \vec{u}_k in terms of the displacement of the surface atoms and obtain after simple algebra

$$\begin{aligned} \sum_{jj'k} \mathbf{K}_{ik} [(\mathbf{G}_{ij} - \mathbf{G}_{ij'}) - (\mathbf{G}_{kj} - \mathbf{G}_{kj'})] \mathbf{K}_{j'j} \vec{u}_j \\ = \sum_k \vec{b}_{ik} + \sum_{jj'k} \mathbf{K}_{ik} (\mathbf{G}_{ij} - \mathbf{G}_{kj}) \vec{b}_{j'j} \end{aligned} \quad (15)$$

Solution of this set of equations gives \vec{u}_j for all surface atoms j . However, the coefficients and constants in the equations require more floating point operations to compute and from actual implementation the equations also take more bi-conjugate gradient steps to solve. This formalism hence is not adopted. On the other hand, the coupling constant in Eq. (15) decays as $1/r^3$ in 3D with the distance r between the corresponding particles. It would be interesting to explore if the steeper decay can lead to a coarsening scheme more efficient than the one to be presented next based on the standard displacement-based formalism.

III. SUPERPARTICLE COARSENING SCHEME

The reduced set of equations (Eq. (10)) from the exact displacement-based Green's function method for obtaining the displacements of the surface atoms and hence the elastic energy greatly speeds up the computation. Yet, it can still be substantially improved using superparticle coarsening approaches used in Refs. [20, 21, 22, 23]. The particular implementation adopted in Refs. [22, 23] will be summarized and more details can be found in Ref. [23]. First, note that the sum over directly connected pairs of real and ghost surface atoms in Eqs. (10) is equivalent to the sums over broken bonds of real surface atoms. We hence rewrite Eq. (10) as

$$\vec{u}_i = \sum_{j\beta} \xi_{j\beta} \left[\Delta \mathbf{G}_{ij\beta} \mathbf{K}_\beta \vec{u}_j - \mathbf{G}_{ij} \vec{b}_\beta \right] \quad (16)$$

where the sum is now over all real surface atoms j and each bond direction β . We put $\xi_{j\beta} = 1$ if the β th bond of atom j is broken and it is 0 otherwise. Also, $\Delta \mathbf{G}_{ij\beta} =$

$G_{ij} - G_{ij'}$, $K_\beta = K_{jj'}$ and $\vec{b}_\beta = \vec{b}_{jj'}$ where the β th bond of atom j is connected directly to atom j' .

The idea of the superparticle approach is as follows. Finding the strain energy ΔE_m of atom m needed in Eq. (1) requires calculating the strain energy E_s of the whole lattice twice with and without atom m . Certain fine details of the surface far away are obviously unimportant and can be neglected. Specifically, surface atoms are grouped into sets called superparticles with the I th of them denoted by Ω_I . We neglect fluctuations within a superparticle by assuming identical displacement $\vec{u}_i \equiv \vec{u}_I$ for each member $i \in \Omega_I$. Equation (16) can then be approximated by

$$\vec{u}_I = \sum_J \left[\mathbf{A}_{IJ} \vec{u}_J - \vec{B}_{IJ} \right] \quad (17)$$

where

$$\mathbf{A}_{IJ} = \sum_{j \in \Omega_J, \beta} \xi_{j\beta} \Delta \mathbf{G}_{Ij\beta} \mathbf{K}_\beta \quad (18a)$$

$$\vec{B}_{IJ} = \sum_{j \in \Omega_J, \beta} \xi_{j\beta} \mathbf{G}_{Ij} \vec{b}_\beta \quad (18b)$$

The index I in \mathbf{G}_{Ij} and $\Delta \mathbf{G}_{Ij\beta}$ denotes the lattice point closest to the centroid of the superparticle Ω_I . At this point, individual constituent particles within the superparticles are still referenced explicitly. To further save computation time, we approximate \mathbf{A}_{IJ} and \vec{B}_{IJ} by

$$\mathbf{A}_{IJ} = \sum_{\beta} n_{J\beta} \Delta \mathbf{G}_{IJ\beta} \mathbf{K}_\beta \quad (19a)$$

$$\vec{B}_{IJ} = \sum_{\beta} n_{J\beta} \mathbf{G}_{IJ} \vec{b}_\beta \quad (19b)$$

respectively. The Green's functions are now completely indexed by the centroid positions I and J while

$$n_{J\beta} = \sum_{j \in \Omega_J} \xi_{j\beta} \quad (20)$$

is the number of broken bonds in superparticle J in direction β . However, Eqs. (19) provide good approximations only when the superparticles I and J are far apart. We still have to use the more accurate Eqs. (18) for superparticles close to each other. In addition, since the problem is always solved in pairs with identical morphology except for one atom m , terms in Eqs. (18) and (19) which remain unchanged in the second calculation are properly re-used. In contrast to conventional methods, the computation time is dominated by the calculations of the coefficients and constants in Eq. (17) using Eqs. (18) and (19) rather than the subsequent iterative solution of the resulting system of equations. At a given coarseness, the number of superparticles scales up roughly as $\log L$ for a substrate with a lateral width L for both 2D and 3D simulations. The computation time which depends on the number of coefficients and constants in Eq. (17) thus scales roughly as $(\log L)^2$. Further details including the grouping of surface atoms into superparticles can be found in Ref. [23].

IV. ATOMIC HOPPING ACCEPTANCE-REJECTION ALGORITHM

Even with the Green's function method and the superparticle approximation, the calculations of the elastic energies of the potentially hopping atoms are still by far the most time consuming parts in the kinetic simulations. We adopt a multi-step hopping algorithm aiming at minimizing the number of these calculations. It can utilize justifiable approximations to improve the computational speed. Yet, by tuning a single parameter Λ to be defined below, it smoothly crosses over and converges back to the original exact hopping algorithm. Therefore, the desired compromise between accuracy and speed can be easily selected to suit a given set of physical conditions. More importantly, impacts of any approximations in the hopping algorithm can be easily accessed by repeating the simulations again with better accuracies.

In the model, each topmost atom is in general allowed to hop to another column simulating the surface diffusion process. The conventional approach is to calculate the hopping rate Γ_m at each column m given by Eq. (1) and then the hopping atom can be randomly sampled according to the associated probabilities. After each successful hopping event, the precise surface configuration changes. Due to the long-range nature of the elastic interactions, ΔE_m and Γ_m for the whole surface in general also change and have to be recomputed. In practice, the elastic interactions are often truncated to a very limited range and thus only values at a small neighborhood require updating [17, 19].

We adopt an alternative acceptance-rejection scheme for efficient sampling of hopping atoms without truncating the elastic interactions. First, as will be explained later, easily computable upper and lower bounds Ω_m^+ and Ω_m^- of ΔE_m are available. Equation (1) then gives an upper bound

$$\Gamma_m^+ = R_0 \exp \left[-\frac{n_{1m}\gamma_1 + n_{2m}\gamma_2 - \Omega_m^+ - E_0}{k_B T} \right] \quad (21)$$

of the rate Γ_m . All values involved are available and Γ_m^+ for the whole surface can be easily kept up-to-date. They are stored in a standard binary tree data structure. At each Monte Carlo step, we first sample m using Γ_m^+ as the relative probability efficiently from the binary tree. Since the upper bound Γ_m^+ instead of the true rate Γ_m is used, atom m hence chosen will hop only with an event acceptance probability

$$p_m = \frac{\Gamma_m}{\Gamma_m^+} = \exp \left[-\frac{\Omega_m^+ - \Delta E_m}{k_B T} \right] \quad (22)$$

It appears that we then need to conduct the intensive computation of ΔE_m to find p_m , but we can do better. A lower bound p_m^- of p_m can easily be obtained from

$$p_m^- = \exp \left[-\frac{\Omega_m^+ - \Omega_m^-}{k_B T} \right] \quad (23)$$

Let ξ be an independent uniform random deviate in $[0, 1)$. If $\xi < p_m^-$, the hopping event is accepted immediately. An explicit calculation of ΔE_m is avoided and this leads to a considerable speed up of the simulation. Otherwise, we finally compute ΔE_m as described in the previous sections in order to calculate p_m in Eq. (22). Using the same random number ξ , the event is accepted if $\xi < p_m$. Otherwise, it is rejected. It can be easily shown that this acceptance-rejection scheme gives the atomic hopping rate in Eq. (1) noting that the time elapsed in a Monte Carlo step is

$$\Delta t = 1 / \sum_m \Gamma_m^+ \quad (24)$$

To calculate the upper and lower bounds required above, we use quick estimates Ω_m of the elastic energies ΔE_m which will be explained in Sec. V. With an estimate Ω_m , we put

$$\Omega_m^+ = \Omega_m + c^+ \quad (25a)$$

$$\Omega_m^- = \Omega_m + c^- \quad (25b)$$

where c^+ and c^- are dynamically calculated global biases. Whenever a calculated value of ΔE_m does not lie within the predicted upper bound Ω_m^+ by a comfortable safety margin Λ taken here as $\Lambda = 0.01eV$, c^+ will be increased considerably to attain a more conservative bound. Otherwise, it is decreased slightly for a more aggressive event acceptance rate. The algorithm for c^- is analogous. We also note that $\Delta E_m \geq 0$ so that Ω_m^- is replaced by 0 if it is negative. For adatoms with elastic couplings neglected, $\Omega_m^+ = \Omega_m^- = \Omega_m = 0$. In case an explicit calculation of ΔE_m is conducted but the hop is finally rejected, we put $\Omega_m^+ = \Omega_m^- = \Delta E_m$ until the next successful hopping event occurs at a neighborhood of m . In particular, for a large safety margin Λ , the algorithm reduces into the original exact one in which all values of ΔE_m has to be explicitly calculated for all topmost atoms after each successful hopping event involving a non-adatom. For small Λ , the algorithm is more efficient but under or over sampling of certain hopping events may occasionally occur.

Our acceptance-rejection hopping algorithm is a multi-step one with a few rather complex components targeting at a good numerical efficiency. It is further complicated by additional special rules such as neglecting the elastic interactions of adatoms and forbidding large atomic steps. Reliable software implementation is non-trivial because minor coding mistakes affecting only certain surface configurations often do not lead to disastrous impacts on the resulting morphology and can be extremely difficult to spot. Hence, we devote great efforts to guarantee a reliable implementation. One particularly helpful consistency check is a Boltzmann's distribution test. Since our model follows detailed balance, an equilibrium surface follows the Boltzmann's distribution. We perform long test simulations of annealing in small lattices with all but two atoms frozen. We make sure that all or most

of the not too many possible configurations will be visited many times. For each configuration, the combined duration should agree with the Maxwell-Boltzmann's distribution within the statistical error bar. We repeat the test with frozen atoms arranged in a wide range of configurations to make sure that hopping events in all circumstances are simulated with the correct probabilities.

V. QUICK ESTIMATES OF ELASTIC ENERGIES

Our hopping algorithms presented in the last section requires an easily computable estimate Ω_m for the elastic energy ΔE_m of each topmost atom m . We now explain our algorithm for generating Ω_m . Consider first simulations in 2D [21]. Due to the assumption of linear elasticity, $\Delta E_m \propto \epsilon^2$. We write

$$\Delta E_m = \epsilon^2 \Phi_m(\{h_i\}_{i=1..L}) \quad (26)$$

where Φ_m is the elastic energy of an atom m extrapolated to unit lattice misfit and it depends on the detailed surface configuration $\{h_i\}_{i=1..L}$ non-trivially. With long-range elastic interactions, ΔE_m and hence Φ_m depend in general on the morphology of the whole surface. We split the surface into a local region \mathcal{L} centered at m and a distant region \mathcal{D} which will be treated accurately and approximately respectively. Given a specific local surface configuration defined in \mathcal{L} , ΔE_m does not only depend on ϵ but also significantly on the morphology in \mathcal{D} . For example, ΔE_m has a much larger magnitude when \mathcal{L} is situated at a highly stressed valley than at a partially relaxed peak. In fact, what is most relevant is the resulting local strain induced by \mathcal{D} averaged over \mathcal{L} . Let λ_m be the horizontal component of this coarsened strain. Analogous to Eq. (26), we hence propose an estimate Ω_m of ΔE_m given by

$$\Omega_m = \lambda_m^2 \Phi(\{h_i\}_{i \in \mathcal{L}}) \quad (27)$$

where the combined effects of the lattice misfit ϵ and the morphology in \mathcal{D} are essentially included in λ_m . Impacts due to microscopic details in \mathcal{D} as well as other strain components are neglected. The elastic energy Φ at unit strain depends non-trivially on the local surface configuration. The local configuration is uniquely characterized by a set of surface steps while the absolute surface height itself is irrelevant. Restricting surface step-heights within $\pm 2a_s$ in the simulations and taking a local region \mathcal{L} of 9 columns wide, there are 8 surface steps and the height of each of them takes one of five allowed values. For each of the 5^8 resulting local configurations, Φ is precomputed and tabulated before the main simulation commences. Specifically, we have used in the precomputation lattices of lateral width $L = 32$. The film thickness at column m is $8a_s$ well cleared of the substrate. In the distant region \mathcal{D} , the thickness equals $16a_s$ uniformly and this generates considerable compression. For every local surface

configuration, the elastic energy ΔE_m is then explicitly calculated using our Green's function approach and Φ is given by $\Delta E_m/\epsilon^2$ which is independent of the misfit ϵ used in the pre-computation.

The coarse-grained local strain λ_m can be estimated easily during the simulation noting that it mainly depends on structural features in \mathcal{D} at a longer length scale and changes relatively slowly. Simply by inverting Eq. (27) and averaging, we obtain

$$\lambda_m^2 = \frac{\langle \Delta E_m \rangle}{\langle \Phi(\{h_i\}_{i \in \mathcal{L}}) \rangle} \quad (28)$$

where $\langle \cdot \rangle$ denotes averaging over data associated with the three most recent explicit calculations of ΔE_m . More precisely, λ_m defined here is consistently smaller than those proportional to the local strain since Φ is precomputed with the local surface located at a valley instead of a flat plane. This however leads to no degradation in the performance as replacing Φ by $c\Phi$ for all local configurations for any constant $c > 0$ leaves our algorithm invariant.

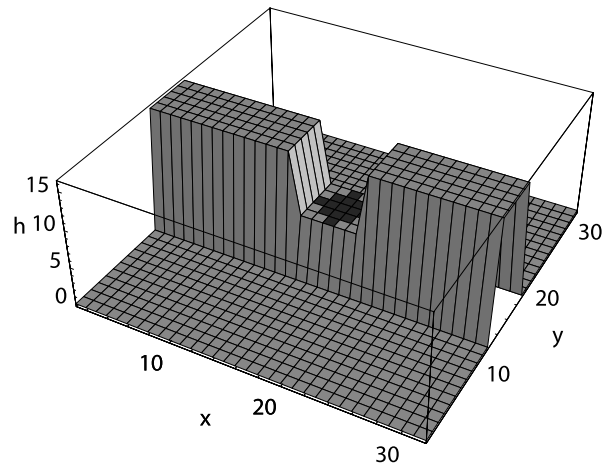


FIG. 2: Film profile in the distant region \mathcal{D} for the precomputation of the strain energy table. The local region \mathcal{L} is shaded in black.

For 3D simulations [22], we generalize Eq. (27) and approximate the elastic energy ΔE_m by

$$\Omega_m = \lambda_{xm}^2 \Phi_x(\{h_i\}_{i \in \mathcal{L}}) + \lambda_{ym}^2 \Phi_y(\{h_i\}_{i \in \mathcal{L}}) \quad (29)$$

where λ_{xm} and λ_{ym} are components of the coarse-grained local strains in planar directions. The local region \mathcal{L} now consists of 13 columns as shown in Fig. 2. Taking into account that step-heights are restricted within ± 1 in our 3D simulations, 3^{12} possible surface configurations characterized by a set of 12 step heights [43] are considered. For each configuration, Φ_x is calculated and tabulated using $\Phi_x = \Delta E_m/\epsilon^2$ which follows from Eq. (29) assuming that the local region is strained only in the x direction with $\lambda_{xm} \simeq \epsilon$ and $\lambda_{ym} \simeq 0$. More precisely, the precomputation is based on films on a $32 \times 32 \times 32$ substrate. The

frozen morphology in the distant region \mathcal{D} is also shown in Fig. 2. It is the simplest morphology which generates a significant strain only in the x direction. Then Φ_y is obtained from Φ_x by symmetry.

In contrast to the 2D case, λ_{xm} and λ_{ym} cannot be solved directly but are instead obtained from a simple least square fit. We define an error measure $\mathcal{E}_m = (\Delta E_m - \Omega_m)^2$. Whenever an explicit calculation of ΔE_m is conducted, the local strain components are updated according to the steepest descent approach as follows

$$\lambda_{xm} \leftarrow \lambda_{xm} - \eta \frac{\partial \mathcal{E}_m}{\partial \lambda_{xm}} \quad (30)$$

$$\lambda_{ym} \leftarrow \lambda_{ym} - \eta \frac{\partial \mathcal{E}_m}{\partial \lambda_{ym}} \quad (31)$$

where the rate constant η is taken as 0.5. Furthermore, λ_{xm} and λ_{ym} are relatively smooth functions of position. To suppress statistical errors, after each steepest descent step, they are further replaced by weighted averages with values at neighboring columns, i.e.

$$\lambda_{xm} \leftarrow w \lambda_{xm} + (1-w) \langle \lambda_{xi} \rangle_m \quad (32)$$

$$\lambda_{ym} \leftarrow w \lambda_{ym} + (1-w) \langle \lambda_{yi} \rangle_m \quad (33)$$

where $w = 0.8$ and $\langle \dots \rangle_m$ denotes averaging over the 8 neighboring columns of site m .

VI. RESULTS

Figure 3 shows an initially flat film from a typical simulation after annealing for $66\mu s$ at a lattice misfit $\epsilon = 6\%$ and temperature $T = 1000K$. Islands have started to form and the roughening mechanism is expected to follow the Asaro-Tiller-Grinfeld instability as explained in Ref. [22]. The nominal thickness is 5 monolayers. The substrate used has $128 \times 128 \times 64$ lattice sites and this is the largest considered in similar kinetic simulations reported in the literature. The pre-computed Green's functions have been calculated for an extended lattice with $128 \times 128 \times (64 + 30)$ sites so that films with a maximum local thickness up to 30 layers can be simulated. Totally, we have carried out 6.5×10^6 hopping attempts (Monte Carlo steps) each of which involves a sampling event according to Eq. (21) based on the upper bound Ω_m^+ of the elastic energy. About 2.2×10^6 of them are successful hops by adatoms with elastic interactions neglected. Of the remaining 4.3×10^6 non-adatom hopping attempts, 1.8×10^6 , i.e. 42% are accepted directly using Eq. (23) based on the lower bound Ω_m^- . In the other 2.5×10^6 attempts, ΔE_m is explicitly computed and a further 0.6×10^6 attempts, i.e. 13% are accepted using Eq. (22). Therefore, a combined 55% of all non-adatom hopping attempts are accepted while the remaining 45% are rejected. Totally, there are hence 4.6×10^6 successful hopping events with 2.4×10^6 of them involving non-adatoms. About 1.04 explicit calculations

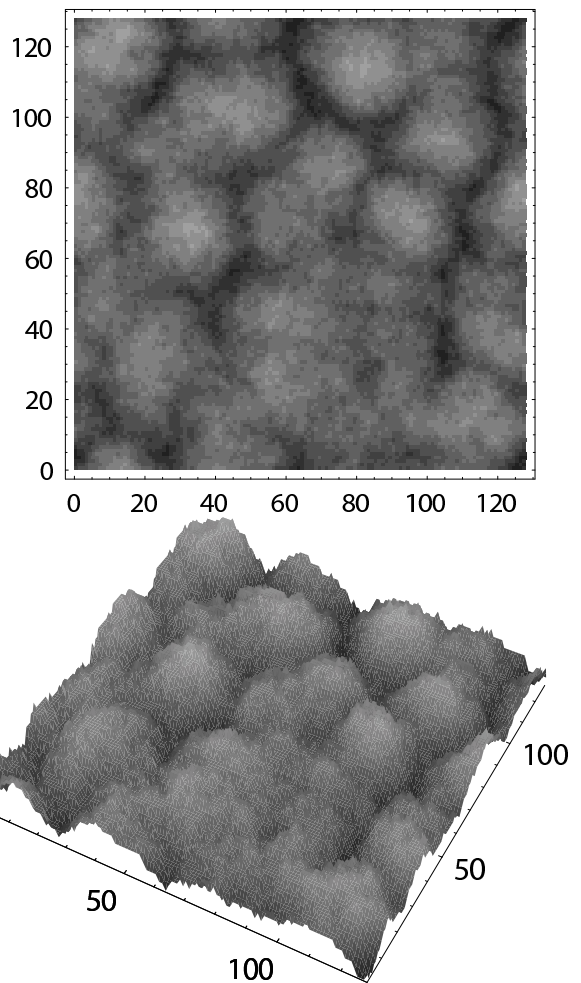


FIG. 3: Surface from a simulation of annealing at misfit $\epsilon = 6\%$ and temperature $T = 1000K$ in top view and 3D view. The peak to peak roughness is 9 monolayers.

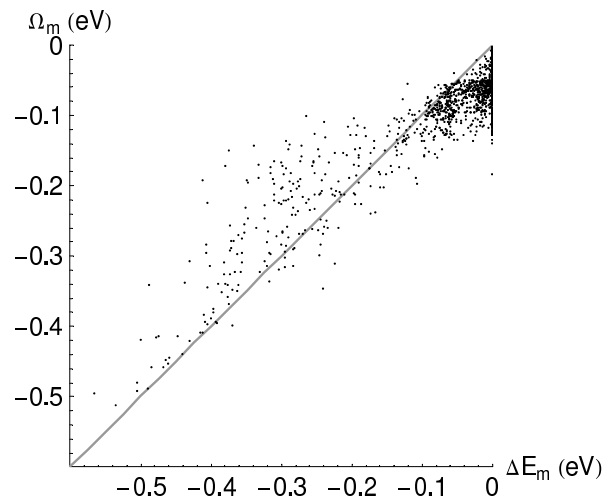


FIG. 4: Plot of Ω_m against ΔE_m where ΔE_m is the elastic energy of a surface atom calculated using the superparticle approach and Ω_m is its quick estimate.

of ΔE_m are carried out for each successful non-atom hopping event compared with nearly 128×128 calculations in principle. Figure 4 plots the quick estimates Ω_m against the more accurate values ΔE_m obtained using the superparticle approximation. The pairs of values are sampled randomly throughout the simulation. For the whole simulation, ΔE_m actually lies outside the predicted bounds only with a small chance of less than 0.8%. The resulting over- or under-samplings of hopping events have shown to be negligible in smaller scale simulations.

The simulations take 18 days to execute on a 2.2GHz Core Duo Pentium computer. The repeated calculations of ΔE_m consume about 85% of the CPU time. We use 110 superparticles. Each calculation takes about 0.5s. About 95% of that goes to computing the coefficients and constants in setting up Eq. (10). This part of our codes have been carefully written to implement both parallel processing with the dual cores and vector processing with arrays each consisting of four single precision floating point numbers provided by the streaming SIMD Extensions 2 (SSE2) of the processor. The Intel C++ compiler is used. The remaining 5% of the computation load is spent on the iterative solution of the equations using the bi-conjugate gradient method. It uses Intel's mathematical kernel library which also takes advantage of the parallel and vector facilities. We use a relatively small tolerance of 0.0001% as the convergence condition for the iterative solution of the superparticle displacements. The overall error in the calculation of the elastic energy ΔE_m is numerically checked to be within about

5% which is essentially due to the superparticle approximation only. The run time of a simulation is expected to scale roughly as $L^2(\log L)^2$ for a substrate with $L \times L$ surface sites. The factors L^2 and $(\log L)^2$ respectively account for the number of hopping surface particles and the computation load for each elastic energy calculation as explained in Sec. III. For instance, when we repeat our simulation using a smaller substrate with $L = 64$, it takes about 3 days to execute.

VII. DISCUSSION

Algorithms for fast Monte Carlo simulation of the morphological evolution of strain heteroepitaxial thin films are presented. A Green's function approach and a superparticle surface coarsening scheme enable efficient calculations of the elastic energies of film atoms. Atomic hopping events following rates in the Arrhenius form are selected using an acceptance-rejection algorithm. The algorithm utilizes estimates of the elastic energies of top-most atoms easily computable from tabulated values for similar local surface configurations after taking into account local strains. With these algorithms, kinetic Monte Carlo simulations have been conducted much more efficiently than it was possible previously.

This work was supported by HK RGC, Grant No. PolyU-5009/06P. LMS is supported by NSF grant DMS 0553487.

-
- [1] V.A. Shchukin and D. Bimberg, Rev. Mod. Phys. **71**, 1125 (1999).
 - [2] P. Politi, G. Grenet, A. Marty, A. Ponchet, and J. Villain, Phys. Rep. **324**, 271 (2000).
 - [3] L.B. Freund and S. Suresh, Thin film materials, stress, defect formation and surface evolution (Cambridge 2003).
 - [4] J. Stangl, V. Holy, and G. Bauer, Rev. Mod. Phys. **76**, 725 (2004).
 - [5] Y.-W. Mo, D.E. Savage, B.S. Swartzentruber, and M.G. Lagally, Phys. Rev. Lett. **65**, 1020 (1990).
 - [6] F.M. Ross, R.M. Tromp, and M.C. Reuter, Science **286**, 1931 (1999).
 - [7] A. Vailionis, B. Cho, G. Glass, P. Desjardins, David G. Cahill, and J. E. Greene, Phys. Rev. Lett. **85**, 3672 (2000).
 - [8] J.A. Floro, E. Chason, L.B. Freund, R.D. Twisten, R.Q. Hwang, and G.A. Lucadamo, Phys. Rev. B **59**, 1990 (1999).
 - [9] R.M. Tromp, F.M. Ross, and M.C. Reuter, Phys. Rev. Lett. **84**, 4641 (2000).
 - [10] P. Sutter and M.G. Lagally, Phys. Rev. Lett. **84**, 4637 (2000).
 - [11] J. Tersoff and F.K. LeGoues, Phys. Rev. Lett. **72**, 3570 (1994).
 - [12] R.J. Asaro and W.A. Tiller, Metall. Trans **3**, 1789 (1972);
 - [13] M.A. Grinfeld, J. Nonlinear Sci. **3**, 35 (1993).
 - [14] D.J. Srolovitz, Acta Metall. **37**, 621 (1989);
 - [15] B. J. Spencer, P.W. Voorhees, and S.H. Davis, J. Appl. Phys. **73**, 4955 (1993).
 - [16] J. Tersoff, B.J. Spencer, A. Rastelli, and H. Von Känel, Phys. Rev. Lett. **89**, 196104 (2002).
 - [17] A. Rastelli, H. Von Känel, B. J. Spencer, and J. Tersoff, Phys. Rev. B, **68**, 115301 (2003).
 - [18] B.G. Orr, D.A. Kessler, C.W. Snyder, and L.M. Sander, Euro. Phys. Lett. **19**, 33 (1992).
 - [19] A.-L. Barabási, Appl. Phys. Lett **70**, 2565 (1997).
 - [20] K.E. Khor and S. Das Sarma, Phys. Rev. B **62**, 16657 (2000).
 - [21] C.H. Lam, C.K. Lee, and L.M. Sander, Phys. Rev. Lett. **89**, 216102 (2002).
 - [22] J.L. Gray, R. Hull, C.H. Lam, P. Sutter, J. Means, and J.A. Floro, Phys. Rev. B **72**, 155323 (2005).
 - [23] M.T. Lung, C.H. Lam, and L.M. Sander, Phys. Rev. Lett. **95**, 086102 (2005).
 - [24] C.H. Lam and M.T. Lung, Int. J. Mod. Phys. B. **21**, 4219 (2007).
 - [25] G. Russo and P. Smereka, J. Comp. Phys. **214**, 809 (2006).
 - [26] G. Russo and P. Smereka, SIAM MMS **5**, 130 (2006).
 - [27] M. Meixner, E. Schöll, V.A. Shchukin, and D. Bimberg, Phys. Rev. Lett. **87**, 236101 (2001).

- [27] R. Zhu, E. Pan, and P. W. Chung, Phys. Rev. B **75**, 205339 (2007).
- [28] W.H. Yang and D.J. Srolovitz, Phys. Rev. Lett. **71**, 1593 (1993).
- [29] Y.W. Zhang, A.F. Bower and P. Liu, Thin Solid Films **424**, 9 (2003).
- [30] P. Liu, Y.W. Zhang, and C. Lu, Phys. Rev. B **68**, 035402 (2003).
- [31] Y. Tu and J. Tersoff, Phys. Rev. Lett. **93**, 216101 (2004); Phys. Rev. Lett. **98**, 096103 (2007).
- [32] Z. Huang, T. Zhou, and C.-h. Chiu, Phys. Rev. Lett. **98**, 196102 (2007).
- [33] F. Much, M. Ahr, M. Biehl and W. Kinzel, Europhys. Lett. **56**, 791 (2001); F. Much and M. Biehl, Europhys. Lett. **63**, 14 (2003).
- [34] M.A. Makeev, W. Yu, and A. Madhukar, Phys. Rev. B **68**, 195301 (2003).
- [35] C. M. Retford, M. Asta, M. J. Miksis, P. W. Voorhees, and E. B. Webb, Phys. Rev. B **75**, 075311 (2007).
- [36] Y. Fujikawa, K. Akiyama, T. Nagao, T. Sakurai, M.G. Lagally, T. Hashimoto, Y. Morikawa, and K. Terakura, Phys. Rev. Lett. **88**, 176101 (2002).
- [37] O. E. Shklyaev, M. J. Beck, M. Asta, M. J. Miksis and P. W. Voorhees, Phys. Rev. Lett. **94**, 176102 (2005).
- [38] G.H. Lu, M. Cuma, and F. Liu, Phys. Rev. B **72**, 125415 (2005).
- [39] D.E. Savage et al, in Semiconductors and Semimetals **56**, R. Hull and J.C. Bean Ed. (Academic Press 1999).
- [40] Eq. (4) corrects a typographical error in Eq. (6) of Ref. [20].
- [41] F. Paris and J. Canas, Boundary element method, fundamentals and applications (Oxford University Press 1997).
- [42] V.K. Tewary, Adv. Phys. **22**, 757 (1973); V.K. Tewary, Phys. Rev. B **69**, 094109 (2004).
- [43] Some of the 3^{12} local configurations uniquely indexed by a selected set of 12 steps actually contain forbidden double-steps and they are assigned null entries in our elastic energy table. This is because there are indeed 16 surface steps between the 13 columns due to the existence of loops on a 2D plane. Explicit knowledge of the exact number of valid configurations however is not needed in our algorithm.